FEBS Letters

FEBS PRESS science publishing by scientists

Model discrimination for Ca^{2+}-dependent regulation of myosin light chain kinase in smooth muscle contraction

Joseph P. Dexter, John W. Biddle and Jeremy Gunawardena

Department of Systems Biology, Harvard Medical School, Boston, MA, USA

Correspondence
J. Gunawardena, Department of Systems Biology, Harvard Medical School, 200 Longwood Avenue, Boston, MA 02115, USA
Fax: +1 617 432 5012
Tel: +1 617 432 4839
E-mail: jeremy@hms.harvard.edu

(Received 6 June 2018, revised 5 July 2018, accepted 11 July 2018, available online 13 August 2018)

doi:10.1002/1873-3468.13207

Edited by Alfonso Valencia

Excitation-contraction coupling in smooth muscle is mediated by the Ca^{2+}- and calmodulin-dependent regulation of myosin light chain kinase. The precise mechanism of this regulation remains controversial, and several mathematical models have been proposed for the interaction of the three species. These models have previously been analyzed at steady state primarily by numerical simulation of differential equations, for which parameter values must be estimated from data. Here, we use the linear framework for timescale separation to demonstrate that models of this general kind can be solved analytically for an equilibrium steady state, without having to determine parameter values. This analysis leads to parameter-independent methods for discriminating between the models, for which we propose experiments that could be performed with existing methods.

Keywords: calcium signaling; calmodulin; excitation-contraction coupling; linear framework; mathematical modeling; myosin light chain kinase

Smooth muscle is nonstriated, involuntary muscle that surrounds hollow organs such as the stomach, intestines, bladder, and uterus. As with skeletal and cardiac muscle, the contraction of smooth muscle is a Ca^{2+}-dependent process [1–3]. The specific mechanisms of contractile regulation, however, are distinct in smooth muscle, which does not contain troponin. In response to various contractile agonists, Ca^{2+} enters the cytosol and binds to the multifunctional protein calmodulin (CaM), which has four Ca^{2+} binding sites, two on the N-terminus and two on the C-terminus (Fig. 1A) [4]. Binding of Ca^{2+}-CaM to myosin light chain kinase (MLCK) induces a conformational change that displaces an autoinhibitory sequence from the MLCK catalytic domain. Activated MLCK then phosphorylates a 20 kD light chain of myosin, which initiates actin/myosin cross-bridge cycling and contraction.

Several theoretical models have been proposed for the interaction of Ca^{2+}, CaM, and MLCK. Binding of Ca^{2+} at either end of CaM is highly cooperative [5–7], and most models therefore assume two binding sites for CaM, one N-terminal and one C-terminal, each of which can bind two Ca^{2+} ions in a single step. Without further restrictions, these assumptions give rise to a ternary model in which $2 \times Ca^{2+}$ and MLCK may bind to CaM in any order ('model 1,' Fig. 1B) [8,9]. Several simplified models have also been suggested on the basis of additional biochemical assumptions. Fajmut *et al.* [10] proposed a six-state model in which Ca^{2+} binding to the C-terminus, but not the N-terminus, obligately precedes binding of MLCK ('model 2,' Fig. 1C), consistent with the order-of-magnitude difference in affinity for Ca^{2+} between the two domains [6,11,12]. Finally, an ordered-sequential mechanism, in which Ca^{2+} must be bound at both the C-terminus and N-terminus of CaM prior to the binding of MLCK, has also been proposed ('model 3,' Fig. 1D) [13]. In addition, variants of these models have been incorporated into much larger reaction networks describing agonist-induced Ca^{2+} mobilization and the physiology of airway smooth muscle [14–16].

There is experimental support for the assumptions of both the full and the truncated models. Activation of MLCK is known to require the binding of four Ca^{2+} to CaM, which was the original justification for the

Abbreviation
CaM, calmodulin; MLCK, myosin light chain kinase.

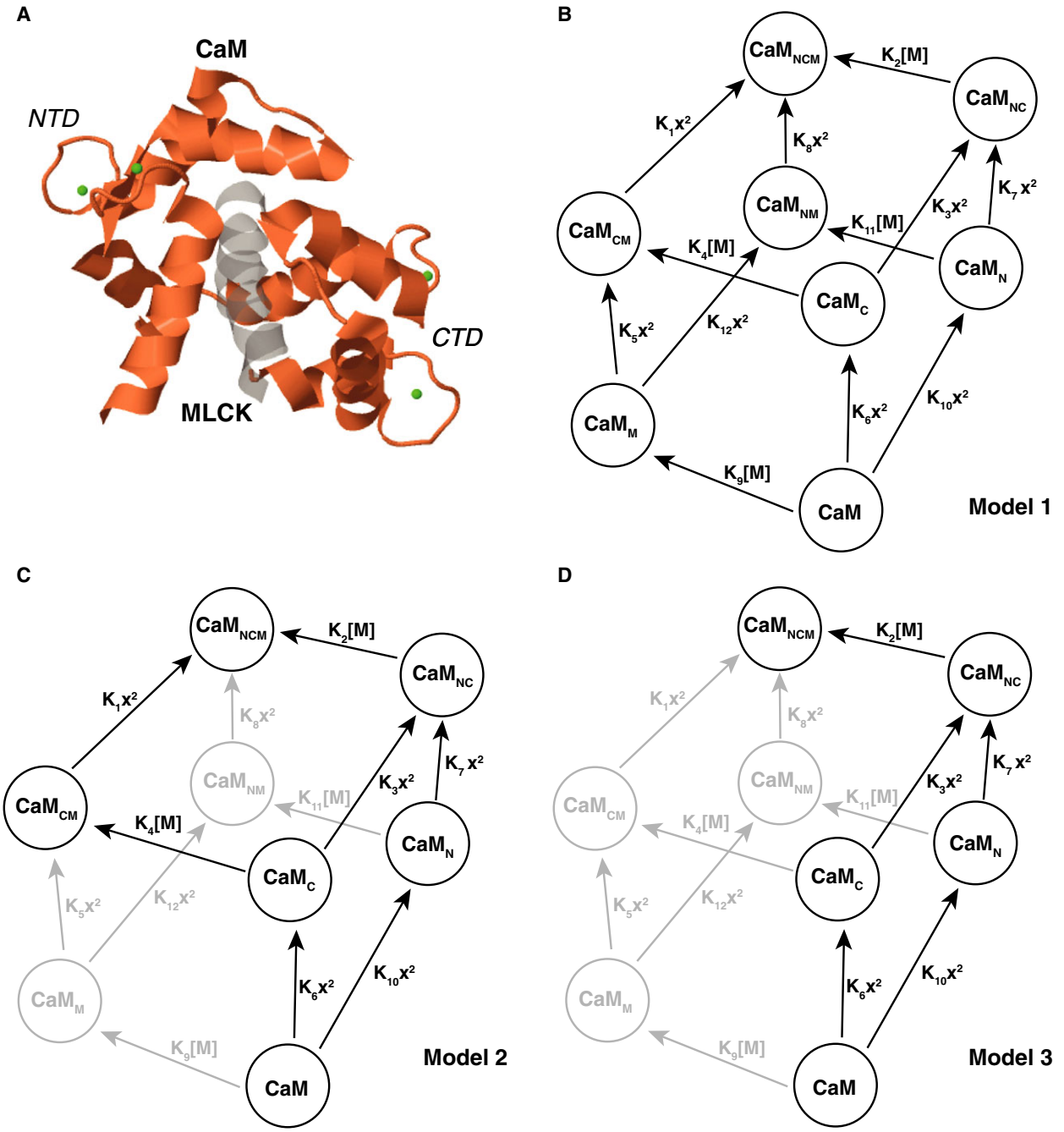

Fig. 1. Proposed models of the Ca^{2+}- and CaM-dependent activation of MLCK. (A) Crystal structure at 1.08 Å resolution of an MLCK peptide (gray) bound to CaM (orange). Two Ca^{2+} (green dots) are bound at the N-terminus and two at the C-terminus. Drawn from data reported by Valentine *et al.* [4]. (B) Equilibrium graph of the eight-state (full) model proposed by Brown *et al.* [8] and Fajmut *et al.* [9]. The notation for equilibrium graphs is described in the text. (C) Equilibrium graph of the six-state model proposed by Fajmut *et al.* [10]. (D) Equilibrium graph of the five-state (sequential) model proposed by Kato *et al.* [13]. The graphs in C and D are truncations of the graph in B; the omitted edges and vertices are colored light gray. In all graphs CaM denotes free calmodulin, and M denotes free MLCK. The subscripts N and C indicate that Ca^{2+} is bound to CaM at the N-terminus and C-terminus, respectively, and the subscript M indicates that MLCK is bound. Free [Ca^{2+}] is denoted by *x*. Two Ca^{2+} ions are assumed to bind CaM simultaneously, following the convention of earlier models.

ordered-sequential model [17,18]. There is mounting evidence, however, that MLCK can bind apo CaM and CaM in complex with two Ca^{2+}, which suggests that the full model or the six-state model might provide a more biochemically realistic description [8,19,20].

Previous analyses of the models have tended to rely on numerical simulation of the systems of ordinary differential equations that arise from the underlying reactions under the assumption of mass-action kinetics. Such simulations require that numerical values be estimated for all parameters in the model. Furthermore, since the binding and unbinding is assumed to take place within a system that is closed overall, without external sources of matter or energy, the steady state is one of thermodynamic equilibrium, so that parameter values must be constrained to satisfy detailed balance. Fajmut *et al.* [9,10] used numerical simulation to calculate the expected fraction of bound to total MLCK at steady state for the full and six-state models, with kinetic parameters drawn from *in vitro* biochemical data in the literature. They found that either model could reproduce an experimental binding curve acquired using a FRET-based sensor [9,10,21]. Kato *et al.* [13] did report a mathematical binding analysis of the simplest (ordered-sequential) model at steady state but did not consider any other models for comparison.

We point out here that it is unnecessary to simulate any of these models to determine their steady-state behavior at thermodynamic equilibrium. Steady states can be calculated analytically without advance knowledge of the numerical values of any parameters. The advantage of such a mathematical analysis, in contrast to numerical simulation, is that it reveals precisely how the steady state depends on the parameters of the system and on the total amounts of the various components. In turn, this information suggests parameter-independent ways in which the different models can be discriminated.

Methods

All conclusions are based on algebraic calculations. A copy of a Mathematica notebook (Wolfram Research, Inc., Champagne, IL, USA, v. 9.0.1.0) containing the main calculations is provided as Supporting Information. The various coefficients that arise from algebraic analysis of the models are listed below. Throughout this section, we denote $CaM_{tot} + M_{tot}$ as T_1 and $CaM_{tot} - M_{tot}$ as T_2.

For model 1, $p_1 = d_1 + d_2x^2 + d_3x^4$ and $p_2 = d_4 + d_5x^2 + d_6x^4 + d_7x^6 + d_8x^8$, with

$$
\begin{aligned}
d_1 &= 1 + K_9T_1\\
d_2 &= K_6(1 + K_4T_1) + K_{10}(1 + K_{11}T_1)\\
d_3 &= K_7K_{10}(1 + K_2T_1)\\
d_4 &= 1 + 2K_9T_1 + K_9^2T_2^2\\
d_5 &= 2\big(K_6\big(1 + K_9T_1 + K_4\big(T_1 + K_9T_2^2\big)\big) + K_{10}\big(1 + K_9T_1\\
&\quad + K_{11}\big(T_1 + K_9T_2^2\big)\big)\big)\\
d_6 &= K_6^2\big(1 + 2K_4T_1 + K_4^2T_2^2\big) + 2K_6K_{10}(1 + K_4T_1\\
&\quad + K_{11}\big(T_1 + K_4T_2^2\big)\big) + K_{10}\big(2K_7\big(1 + K_2T_1 + K_9\big(T_1 + K_2T_2^2\big)\big)\\
&\quad + K_{10}\big(1 + 2K_{11}T_1 + K_{11}^2T_2^2\big)\big)\\
d_7 &= 2K_7K_{10}\big(K_6\big(1 + K_4T_1 + K_2\big(T_1 + K_4T_2^2\big)\big) + K_{10}\big(1 + K_2T_1\\
&\quad + K_{11}\big(T_1 + K_2T_2^2\big)\big)\big)\\
d_8 &= K_7^2K_{10}^2\big(1 + 2K_2T_1 + K_2^2T_2^2\big).
\end{aligned}
$$

For model 2, $p_3 = d_9 + d_{10}x^2 + d_{11}x^4$ and $p_2 = d_{12} + d_{13}x^2 + d_{14}x^4 + d_{15}x^6 + d_{16}x^8$, with

$$
\begin{aligned}
d_9 &= 1\\
d_{10} &= K_6(1 + K_4T_1) + K_{10}\\
d_{11} &= K_7K_{10}(1 + K_2T_1)\\
d_{12} &= 1\\
d_{13} &= 2(K_6(1 + K_4T_1) + K_{10})\\
d_{14} &= K_6^2\big(1 + 2K_4T_1 + K_4^2T_2^2\big) + 2K_{10}\big(K_6\big(1 + K_4T_1\big)\\
&\qquad + K_7\big(1 + K_2T_1\big)\big) + K_{10}^2\\
d_{15} &= 2K_7K_{10}\big(K_6\big(1 + K_4T_1 + K_2\big(T_1 + K_4T_2^2\big)\big) + K_{10}\big(1 + K_2T_1\big)\\
d_{16} &= K_7^2K_{10}^2\big(1 + 2K_2T_1 + K_2^2T_2^2\big).
\end{aligned}
$$

For model 3, $p_5 = d_{17} + d_{18}x^2 + d_{19}x^4$ and $p_6 = d_{20} + d_{21}x^2 + d_{22}x^4 + d_{23}x^6 + d_{24}x^8$, with

$$
\begin{aligned}
d_{17} &= 1\\
d_{18} &= K_6 + K_{10}\\
d_{19} &= K_7K_{10}(1 + K_2T_1)\\
d_{20} &= 1\\
d_{21} &= 2(K_6 + K_{10})\\
d_{22} &= 2K_{10}(K_6 + K_7(1 + K_2T_1)) + K_6^2 + K_{10}^2\\
d_{23} &= 2K_7K_{10}(1 + K_2T_1)(K_6 + K_{10})\\
d_{24} &= K_7^2K_{10}^2\big(1 + 2K_2T_1 + K_2^2T_2^2\big).
\end{aligned}
$$

For model 1 with impaired N-terminal Ca^{2+} binding, $p_7 = d_{25} + d_{26}x^2$ and $p_8 = d_{27} + d_{28}x^2 + d_{29}x^4$, with

$$
\begin{aligned}
d_{25} &= 1 + K_9T_1\\
d_{26} &= K_6(1 + K_4T_1)\\
d_{27} &= 1 + 2K_9T_1 + K_9^2T_2^2\\
d_{28} &= 2K_6\big(1 + K_9T_1 + K_4\big(T_1 + K_9T_2^2\big)\big)\\
d_{29} &= K_6^2\big(1 + 2K_4T_1 + K_4^2T_2^2\big).
\end{aligned}
$$

For model 2 with impaired N-terminal Ca^{2+} binding, $p_9 = d_{30} + d_{31}x^2$ and $p_{10} = d_{32} + d_{33}x^2 + d_{34}x^4$, with

$$d_{30} = 1$$
$$d_{31} = K_6(1 + K_4T_1)$$
$$d_{32} = 1$$
$$d_{33} = 2K_6(1 + K_4T_1)$$
$$d_{34} = K_6^2(1 + 2K_4T_1 + K_4^2T_2^2).$$

Results

Equilibrium binding analysis of three models of Ca^{2+}- and CaM-dependent activation of MLCK

Our mathematical analysis relies on the graph-based linear framework for timescale separation developed in [22,23], which should be consulted for more details; for a review, see [24], and for other applications, see [25–27]. Briefly, the framework can be applied to a timescale separation, in which a subsystem is taken to operate sufficiently fast with respect to its environment that it can be assumed to have reached steady state. The steady-state assumption is then used to eliminate the components of the subsystem, in the sense of expressing their steady-state concentrations in terms of the parameters and the concentrations of components in the environment that may be interacting with the subsystem. Steady states may either be at thermodynamic equilibrium within a closed system or away from thermodynamic equilibrium in an open system [26]. Here, the subsystem is taken to be the various forms of CaM, the steady state is one of thermodynamic equilibrium, and it is the steady-state concentrations of these forms that are to be determined.

Biochemical reactions typically give rise to nonlinear dynamics, as is the case for binding reactions. However, this nonlinear dynamics can sometimes be rewritten as a linear dynamics arising from a graph with directed edges and labels on the edges [22]. Such a graph for model 1 resembles that shown in Fig. 1B, but its edges and labels have been simplified to reflect thermodynamic equilibrium, as explained below. The vertices of the graph represent the components of the subsystem (the different forms of CaM), while the edges represent the biochemical reactions that interconvert these components through interaction with components in the environment outside the subsystem. The nonlinearity is incorporated into the edge labels, which may be complex expressions containing both typical parameters, such as rate constants, as well as the free concentrations of the interacting components in the environment. Here, these interacting environmental components are Ca^{2+} and MLCK, whose free concentrations are denoted in the graph by x and [M], respectively.

The linear dynamics arising from the graph is common to all applications of the linear framework. In contrast, the nonlinearity in the labels must be dealt with in different ways depending on the specific application. Here, a conservation law for the total amount of MLCK, denoted M_{tot}, is used to determine the free concentration of MLCK, while it is assumed as an approximation that the free concentration of Ca^{2+} does not change as a result of binding. In this case, the free concentration of Ca^{2+} is effectively the same as its total concentration. This approximation is reasonable if the number of free molecules is large compared to the number bound, as is typical in an *in vitro* binding assay, and has been used in all previous studies [9,10,13].

Since only the steady state is analyzed here, it is not necessary to write down the linear dynamics that governs the approach to the steady state. Provided that the linear framework graph is strongly connected, so that any two vertices can be joined by a contiguous path of directed edges, the steady state is unique up to a scalar factor. Thermodynamic equilibrium implies reversibility of the graph, so that, if there is an edge between any two vertices, there is also a reverse edge between the same vertices in the opposite direction [22]. Accordingly, as long as the graph is not broken into two separate parts, which is never the case here, it must always be strongly connected. In particular, the graphs shown in the figures are all strongly connected, although this may not be immediately apparent because, as explained below, only the edge in the direction of binding is shown. A specific steady state can be calculated from the structure of the graph in terms of the edge labels. The unknown scalar factor is removed by normalizing to the total concentration of material in the graph, which in the present case is the total amount of CaM, denoted CaM_{tot}. The normalization to CaM_{tot} gives rise to the typical algebraic structure for the steady state of each component of the subsystem, as a rational expression in the edge labels.

A second conservation law describes how CaM_{tot} is composed from the various forms of CaM represented by the vertices of the graph. The interplay between the conservation laws for M_{tot} and CaM_{tot} resolves the remaining nonlinearities in the system, as we will see below.

If the steady state is one of thermodynamic equilibrium, as it is for the models considered here, then the steady state is equivalent to what is derived from equilibrium statistical mechanics [22]. The linear framework makes it unnecessary to have familiarity with this branch of physics but, for those readers who do, we note that the denominator in the rational

expressions corresponds to the partition function. (One of the advantages of the linear framework is that it can also be applied away from thermodynamic equilibrium [27].) For binding and unbinding reactions at thermodynamic equilibrium, the steady state depends only on the association constants, given by the ratio of the binding on-rate to the unbinding off-rate [26,27]. Accordingly, the linear framework graphs in this paper have been simplified to show a single edge in the direction of binding, labeled with the ratio of the binding label to the unbinding label.

In more detail, Fig. 1B shows the simplified linear framework graph for the model of Fajmut *et al.* [9] (model 1). CaM is assumed to have two sites for binding of $2 \times Ca^{2+}$ and one site for binding of M, so that there are $2^3 = 8$ vertices in the graph. The association constants for binding of Ca^{2+} and M are denoted K_1, ⋯, K_{12}. The graphs for models 2 and 3 are truncations of the graph for model 1, as shown in Fig. 1C,D (omitted vertices and edges are colored light gray). Throughout the following analysis, we use square brackets to denote concentration at steady state.

The labeling we have used is particularly convenient for calculating steady states, for which there is a simple rule at thermodynamic equilibrium. For instance, taking the unbound form of CaM as the reference vertex, the steady-state concentration of any vertex can be calculated from [CaM] by choosing any contiguous path of directed edges from CaM to that vertex and multiplying the labels along the path. For instance, taking the path from CaM to CaM_N to CaM_{NC} to CaM_{NCM}, the steady-state concentration of the active complex, CaM_{NCM}, is given by

$$[\mathrm{CaM_{NCM}}] = \left(K_2 K_7 K_{10} [\mathrm{M}] x^4\right) [\mathrm{CaM}].$$

There are, of course, many paths from which to choose. It is a consequence of thermodynamic equilibrium that all such paths give the same result, which implies relationships among the equilibrium constants that arise from detailed balance and the cycle condition [22]. For instance, taking instead the path from CaM to CaM_M to CaM_{CM} to CaM_{NCM}, we see that detailed balance requires

$$K_2 K_7 K_{10} = K_1 K_5 K_9.$$

It is not necessary to impose these relationships for the calculations made below, but they can always be used to reorganize the resulting formulas using association constants found on equivalent paths.

It is now straightforward to write down analytic expressions for two quantities of potential experimental interest, the ratio of the active complex (CaM_{NCM}) to M_{tot}, which we call A_1, and the ratio of all bound MLCK to M_{tot}, which we call F_1. These two quantities are the focus of previous computational analyses [3,9,10]. For the full model, we have the following two conservation laws:

$$\begin{aligned}\mathrm{CaM_{tot}} &= [\mathrm{CaM}] + [\mathrm{CaM_M}] + [\mathrm{CaM_N}] + [\mathrm{CaM_C}] \\ &\quad + [\mathrm{CaM_{NM}}] + [\mathrm{CaM_{CM}}] + [\mathrm{CaM_{NC}}] + [\mathrm{CaM_{NCM}}] \\ &= [\mathrm{CaM}](1 + A(x) + B(x)[\mathrm{M}]),\end{aligned} \tag{1}$$

and

$$\begin{aligned}\mathrm{M_{tot}} &= [\mathrm{M}] + [\mathrm{CaM_M}] + [\mathrm{CaM_{NM}}] + [\mathrm{CaM_{CM}}] + [\mathrm{CaM_{NCM}}] \\ &= [M](1 + B(x)[\mathrm{CaM}]),\end{aligned} \tag{2}$$

where

$$\begin{aligned}A(x) &= (K_6 + K_{10})x^2 + K_7 K_{10} x^4 \\ B(x) &= K_9 + (K_4 K_6 + K_{10} K_{11})x^2 + K_2 K_7 K_{10} x^4.\end{aligned}$$

For convenience, the combined expressions $A(x)$ and $B(x)$ are used throughout the analysis of the different models. Thus, after canceling [M], we have

$$A_1 = \frac{[\mathrm{CaM_{NCM}}]}{\mathrm{M_{tot}}} = \frac{K_2 K_7 K_{10} x^4 [\mathrm{CaM}]}{1 + B(x)[\mathrm{CaM}]}, \tag{3}$$

and

$$F_1 = \frac{\mathrm{M_{bound}}}{\mathrm{M_{tot}}} = \frac{B(x)[\mathrm{CaM}]}{1 + B(x)[\mathrm{CaM}]}. \tag{4}$$

Equations (3,4) are expressed in terms of [CaM], which is difficult to measure or manipulate directly in an experiment. We can, however, determine this quantity using the conservation law for total CaM (Eqn 1). Equations (1,2) are both independently of first order in [CaM] and in [M] (since MLCK binds only once to CaM), despite being highly nonlinear in x. It is therefore straightforward to solve these equations for [CaM] and [M] in terms of x. We find that [CaM] satisfies a quadratic equation,

$$[\mathrm{CaM}]^2 + b_1 [\mathrm{CaM}] + c_1 = 0, \tag{5}$$

whose coefficients can be expressed in terms of x as

$$\begin{aligned}b_1 &= \frac{1 + A(x) + B(x)(\mathrm{M_{tot}} - \mathrm{CaM_{tot}})}{(1 + A(x))B(x)} \\ c_1 &= -\frac{\mathrm{CaM_{tot}}}{(1 + A(x))B(x)}.\end{aligned}$$

A quadratic equation of the form shown in Eqn (5) has a single positive real root, along with a single

negative real root, if, and only if, its constant term is negative. $A(x)$ and $B(x)$ are positive for all positive values of the equilibrium constant and of x, so Eqn (5) has one positive real root. (The negative real root is not meaningful for the analysis.) Substituting the positive root into Eqn (3) gives, as a function of x,

$$A_1(x) = \frac{2K_2K_7K_{10}\mathrm{CaM_{tot}}x^4}{p_1 + \sqrt{p_2}}, \tag{6}$$

where

$$p_1 = d_1 + d_2x^2 + d_3x^4$$
$$p_2 = d_4 + d_5x^2 + d_6x^4 + d_7x^6 + d_8x^8.$$

Here, d_1, ⋯, d_8 are algebraic expressions in the equilibrium constants and the conserved totals. Throughout the paper, the full expressions for coefficients of this kind are listed in the Methods, with the details of their calculation provided in a Supporting Mathematica notebook.

Similarly, we have

$$F_1(x) = \frac{2B(x)\mathrm{CaM_{tot}}}{p_1 + \sqrt{p_2}}. \tag{7}$$

Equations (6,7) give A_1 and F_1 as functions of x, in terms of the Ks and the conserved totals ($\mathrm{CaM_{tot}}$ and $\mathrm{M_{tot}}$). The free concentrations of CaM and MLCK, which are inaccessible to measurement, have been eliminated.

Models 2 and 3 can be analyzed in an identical fashion, so that we have

$$A_2(x) = \frac{2K_2K_7K_{10}\mathrm{CaM_{tot}}x^4}{p_3 + \sqrt{p_4}},$$

and

$$F_2(x) = \frac{2\mathrm{CaM_{tot}}\left(K_4K_6x^2 + K_2K_7K_{10}x^4\right)}{p_3 + \sqrt{p_4}},$$

where p_3 and p_4 have the same algebraic form as p_1 and p_2, respectively. For model 3, there is only a single complex with MLCK bound ($\mathrm{CaM_{NCM}}$) and therefore no distinction between A and F. We have

$$A_3(x) = F_3(x) = \frac{2K_2K_7K_{10}\mathrm{CaM_{tot}}x^4}{p_5 + \sqrt{p_6}},$$

where p_5 and p_6 again have the same algebraic form as p_1 and p_2, respectively.

These algebraic expressions for $A_1(x)$, $A_2(x)$, and $A_3(x)$ and for $F_1(x)$, $F_2(x)$, and $F_3(x)$ can be used to calculate the dependence of MLCK activation and binding on x. Figure 2 shows plots of $A(x)$ and $F(x)$ for the three models, assuming the reference values for K_1, ⋯, K_{12} given in Fajmut *et al.* [9] and setting $\mathrm{M_{tot}} = \mathrm{CaM_{tot}} = 2$ μM.

The curves in Fig. 2 are the primary predictions reported in Fajmut *et al.* [9,10] from numerical simulation of the underlying systems of ordinary differential equations. As we have shown here, numerical simulation is not required, and the functional form of steady-state quantities like A and F may be calculated with the K parameters and the conserved totals treated symbolically. Parameter values need only be estimated to plot the expressions for A and F calculated above, as in Fig. 2.

Parameter-independent criteria for model discrimination

A main goal of our analysis is to identify a minimal set of experimental tests that could distinguish between the three proposed models of MLCK activation, without recourse to numerical fitting of parameter values. For reasons of experimental convenience that will be discussed in greater detail below, our analysis here focuses on the predicted F ratios (i.e., fraction of MLCK bound). We propose a two-step approach that could first differentiate model 1 from models 2 and 3 and then differentiate model 3 from models 1 and 2.

We note that there is a constant term (i.e., a term that is not dependent on x) in the numerator of F_1 but not of F_2 and F_3. Setting $x = 0$ in the relevant expressions, we find that

$$F_1(0) = \frac{2K_9\mathrm{CaM_{tot}}}{1 + K_9(\mathrm{M_{tot}} + \mathrm{CaM_{tot}}) + \sqrt{1 + 2K_9(\mathrm{CaM_{tot}} + \mathrm{M_{tot}}) + K_9^2(\mathrm{CaM_{tot}} - \mathrm{M_{tot}})^2}}, \tag{8}$$

which is evidently positive, while

$$F_2(0) = F_3(0) = 0.$$

This difference is illustrated in Fig. 2B, where models 2 and 3, but not model 1, shows vanishingly low levels of bound MLCK at $x < 10$ nM. (The approximation we have made of treating x as equal to the total concentration of Ca^{2+} may break down at such low levels, but the discrepancy works in our favor here because x must always be less than the

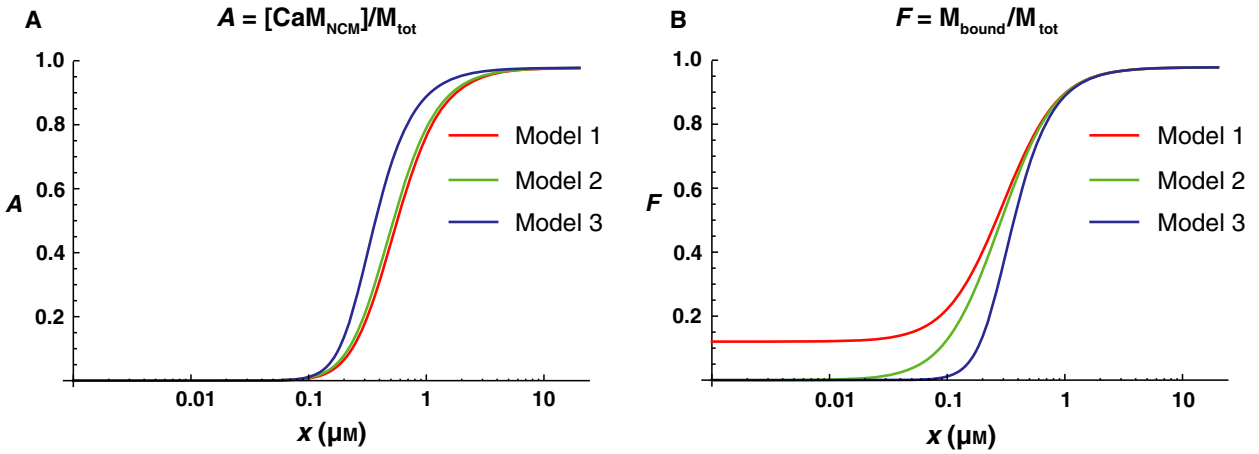

Fig. 2. Binding curves for the three models. K_1, ⋯, K_{12} were set to the reference values given in Fajmut *et al.* [9], and M_{tot} and CaM_{tot} were both set to 2 μM. (A) Fraction of active MLCK (CaM_{NCM}) as a function of x for the three models in Fig. 1. (B) Fraction of bound MLCK as a function of x for the three models in Fig. 1.

total concentration). Assuming the parameter values and initial conditions used in previous numerical simulations [9], we calculate that, according to model 1, ~ 12% of MLCK would be bound to CaM in 1 nM Ca^{2+}, compared to less than 0.01% according to models 2 or 3. It is also clear from Eqn (8) that, for positive values of CaM_{tot}, M_{tot}, and K_9, $F_1(0)$ is an increasing function of CaM_{tot}, so that its value can be increased by raising the level of total CaM. For their simulations, Fajmut *et al.* [9] set M_{tot} =CaM_{tot} = 2 μM, but, with M_{tot} = 2 μM and CaM_{tot} = 20 μM, ~ 59% of MLCK would be bound at x = 1 nM according to model 1. Thus, an experimental test of model 1 could involve measurement of MLCK binding in a Ca^{2+}-free buffer, with CaM available in large excess over MLCK.

Furthermore, Eqn (8) shows that $F_1(0)$ depends on the single equilibrium constant (K_9), which Fajmut *et al.* [9] set to 0.078 μM^{-1} after consideration of several experimental measurements [8,14,28]. The experimental values reported, however, vary over several orders of magnitude, from 0.0037 to 1 μM^{-1}. For any value of K_9 within this range, it is still possible to discriminate model 1 from models 2 and 3 by measuring MLCK binding in low Ca^{2+}; for instance, with K_9 = 0.0037 μM^{-1}, M_{tot} = 2 μM, CaM_{tot} = 20 μM, and x = 10 nM, we calculate from model 1 that ~ 7% of MLCK would be bound, compared to negligible levels according to models 2 and 3. Of course, the fraction bound could be increased by having total CaM in even larger excess.

If model 1 were falsified by the above test, it would then be necessary to distinguish between models 2 and 3, which is challenging to do on the basis of the binding of wild-type CaM to MLCK. For a CaM mutant with impaired Ca^{2+} binding at the N-terminus, however, we can give a parameter-independent criterion to differentiate between the corresponding models 2 and 3. Figure 3 shows three additional graphs, corresponding to models 1, 2, and 3, respectively, for a mutant that is unable to bind Ca^{2+} at its N-terminus. The fraction of bound MLCK for model 1 of the mutant, denoted with a superscript asterisk, is given by

$$F_1^*(x) = \frac{2\mathrm{CaM_{tot}}\left(K_9 + K_4K_6x^2\right)}{p_7 + \sqrt{p_8}},$$

where p_7 is a polynomial in x of degree two and p_8 a polynomial in x of degree four, whose coefficients are combinations of the equilibrium constants, M_{tot}, and CaM_{tot}. Similarly, we have

$$F_2^*(x) = \frac{2K_4K_6\mathrm{CaM_{tot}}x^2}{p_9 + \sqrt{p_{10}}},$$

where p_9 and p_{10} have the same algebraic structure as p_7 and p_8, respectively. For model 3, however, there are no longer any reactions involving MLCK binding, so self-evidently

$$F_3^*(x) = 0. \tag{9}$$

For models 1 and 2, MLCK binding is maximized in the high Ca^{2+} limit, for which we have

$$\lim_{x\to\infty} F_1^* = \lim_{x\to\infty} F_2^* = \frac{2K_4\mathrm{CaM_{tot}}}{1+K_4(\mathrm{CaM_{tot}}+\mathrm{M_{tot}})+\sqrt{1+2K_4(\mathrm{CaM_{tot}}+\mathrm{M_{tot}})+K_4^2(\mathrm{CaM_{tot}}-\mathrm{M_{tot}})^2}}. \quad (10)$$

As such, we calculate, assuming the reference parameter values, that ~ 84% of MLCK would be bound in 1 mM Ca^{2+}, which could be increased to 99% by increasing CaM_{tot} to 20 μM. In the reference parameter set, K_4 = 16.7 μM^{-1} on the basis of a single experimental measurement [8], and K_6 = 0.47 μM^{-2}, which is on the low end of a range of empirical values considered by Fajmut *et al.* [9]. Even with both parameters decreased by three orders of magnitude, models 1 and 2 still predict 25% binding, assuming M_{tot} = 2 μM, CaM_{tot} = 20 μM, and x = 1 mM. Accordingly, the second discrimination test could involve measurement of MLCK binding in a high concentration of Ca^{2+}, with mutant CaM in excess over MLCK.

$$F = \frac{[\mathrm{CaM_M}]}{[\mathrm{M}]+[\mathrm{CaM_M}]}$$

and the following two conservation laws:

$$\mathrm{CaM_{tot}} = [\mathrm{CaM}]+[\mathrm{CaM_M}] \quad (11)$$

and

$$\mathrm{M_{tot}} = [\mathrm{M}]+[\mathrm{CaM_M}]. \quad (12)$$

Equations (11,12) together define a quadratic equation in [CaM], which, as before, can be used to eliminate [CaM] from the expression for F. Following the same procedure as for analysis of the full model, we find,

$$F = \frac{[\mathrm{CaM_M}]}{\mathrm{M_{tot}}} = \frac{2K\mathrm{CaM_{tot}}}{1+K(\mathrm{CaM_{tot}}+\mathrm{M_{tot}})+\sqrt{1+2K(\mathrm{CaM_{tot}}+\mathrm{M_{tot}})+K^2(\mathrm{CaM_{tot}}-\mathrm{M_{tot}})^2}},$$

Limiting behavior of the models in low and high Ca^{2+}

In the previous section, we derived expressions for the fraction of MLCK bound in zero Ca^{2+} (for model 1) and in the high Ca^{2+} limit (for models 1 and 2 with an N-terminal mutant). Equations (8,10) have identical algebraic structure, with the sole difference being the equilibrium constant that appears in the expression. This similarity is not coincidental. In both limits, the reaction network effectively reduces to a bimolecular reaction. In the first (zero Ca^{2+}) case, this reaction involves MLCK and apo CaM, so we have following two-vertex truncation of the graph in Fig. 1:

$$\mathrm{CaM} \overset{K_9[\mathrm{M}]}{\rightleftharpoons} \mathrm{CaM_M}.$$

For the second (high Ca^{2+}) case, we have the following truncation of the graph in Fig. 3:

$$\mathrm{CaM} \overset{K_4[\mathrm{M}]}{\rightleftharpoons} \mathrm{CaM_M}.$$

In both instances, there is only a single complex involving MLCK (CaM_M), so we have where $K = K_9$ in the first case and $K = K_4$ in the second. This calculation explains why the limiting formulas in Eqns (8,10) have the same algebraic structure.

Discussion

The main predictions of our mathematical analysis are in principle testable using existing experimental technology. Several FRET-based biosensors have been developed for monitoring the binding of Ca^{2+}-CaM to MLCK. These sensors typically consist of two variants of green fluorescent protein tethered by the MLCK binding sequence from CaM, so that binding of Ca^{2+}-CaM disrupts interaction between the fluorescent protein pair and reduces FRET [21,29,30]. Such sensors have enabled the characterization of MLCK localization and binding in a number of cell culture systems, as well as *in vivo* using a transgenic biosensor mouse [30–32]. Of particular interest, Geguchadze *et al.* [21] showed that sensor fluorescence tracked phosphorylation of the myosin regulatory light chain in HEK-293T cells, suggesting that their sensor might be useful for quantitative profiling of MLCK activation.

Following the analysis presented in the previous section, failure to detect binding of CaM to MLCK in the

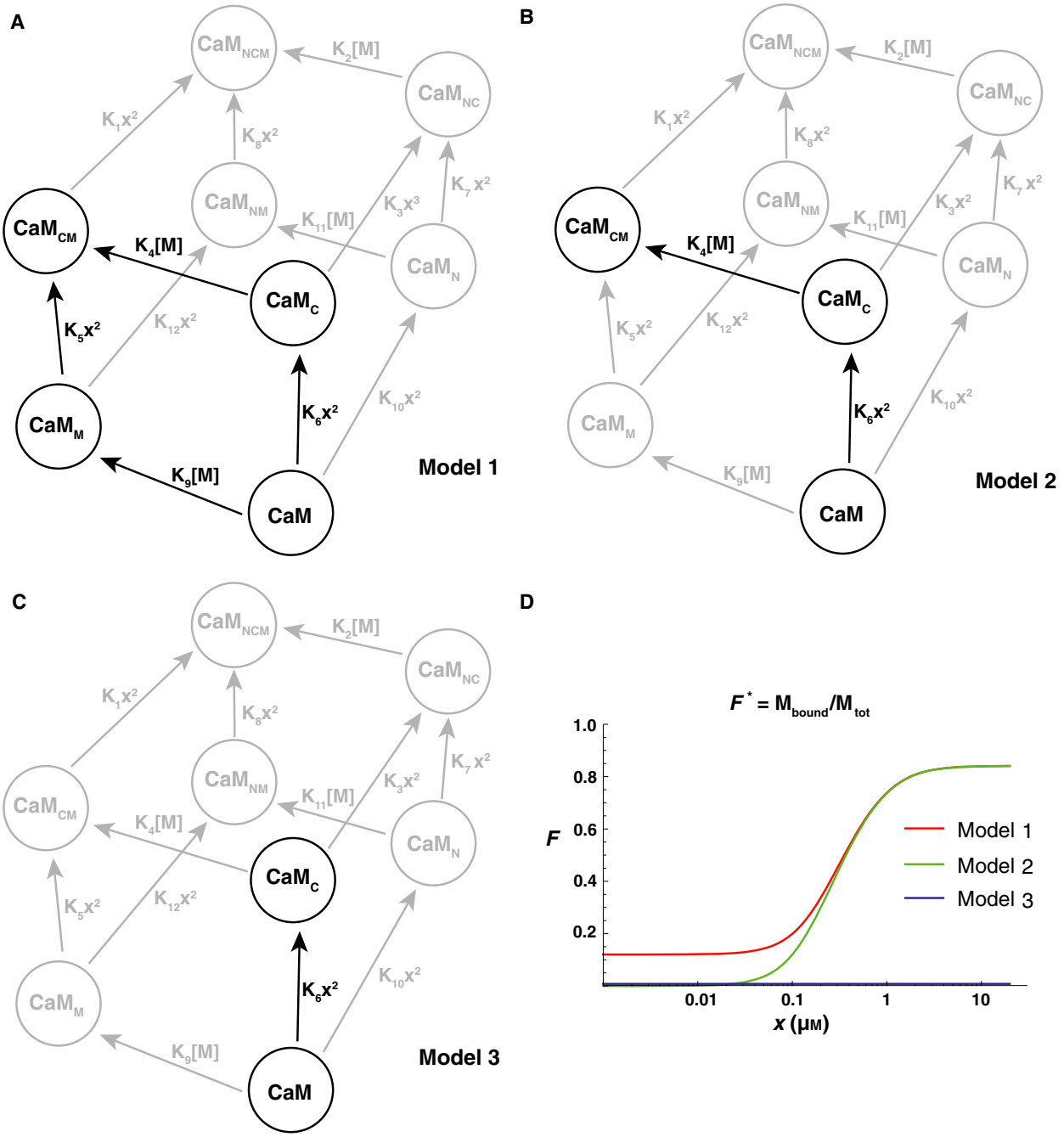

Fig. 3. Comparison of the three models for CaM mutant with impaired Ca^{2+} binding at the N-terminus. (A) Equilibrium graph of the eight-state (full) model proposed by Fajmut *et al.* [9] for mutant. (B) Equilibrium graph of the six-state model proposed by Fajmut *et al.* [10] for mutant. (C) Equilibrium graph of the five-state (sequential) model proposed by Kato *et al.* [13] for mutant. The notation follows Fig. 1. (D) Fraction of bound MLCK as a function of x for the three models for mutant CaM. Note that, in view of Eqn (9), the curve for model 3 is coincident with the horizontal axis. The parameter values are the same as for Fig. 2.

absence of Ca^{2+} would be sufficient to falsify model 1. Such an experiment could be performed using any of the previously developed biosensors, ideally *in vitro* with purified sensor and CaM (so as to maintain as precise control as possible over the Ca^{2+} concentration in the buffer). As detailed above, assuming the reference parameter values in Fajmut *et al.* [9], we calculate according to model 1 that ~ 12% of MLCK would be bound to CaM in 1 nM Ca^{2+} (compared to less than 0.01% for models 2 or 3), a difference which is readily

detectable using existing sensors [9,21]. There is already limited experimental evidence against model 1; in lysates of cells stably expressing their biosensor, Geguchadze *et al*. [21] observed no binding at $x = 2.5$ nM.

Discriminating between models 2 and 3 would require binding measurements with a mutant CaM that exhibits impaired Ca^{2+} binding at the N-terminus. The structural and functional properties of CaM have been studied extensively by site-directed mutagenesis, and there are standard strategies for disabling CaM EF hands without major disruption to the rest of the protein [33,34]. For an appropriate mutant (such as D20A and D56A for human CaM), measurement of non-negligible binding at any reasonably high x would be sufficient to falsify model 3, completing the two-step model discrimination strategy.

Our analysis thus demonstrates that the three models, notwithstanding their numerous similarities, give rise to distinct, experimentally testable predictions about the systems's steady-state behavior. In contrast to previous computational studies of MLCK activation, these predictions are based entirely on algebraic calculations that treat the equilibrium constants symbolically. Inspection of the analytic formulas resulting from these calculations enabled us to identify predictions that are true regardless of the precise numerical values of the parameters, which could not be achieved from numerical simulation alone. In addition to clarifying the relationship between proposed models of CaM/MLCK interaction, variants of our approach should be useful for discriminating between unordered and ordered binding models in diverse physiological contexts.

Acknowledgements

We thank Aldebaran Hofer, Yasemin Sancak, and Felix Wong for helpful discussions and comments on the manuscript. JPD was supported by a NSF Graduate Research Fellowship (DGE1144152), and JWB and JG were supported by NSF grant 1462629.

Author contributions

JPD and JG designed research; JPD, JWB and JG performed research; and JPD and JG wrote the manuscript.

References

1 Webb RC (2003) Smooth muscle contraction and relaxation. *Adv Physiol Educ* **27**, 201–206.

2 Hong F, Haldeman BD, Jackson D, Carter M, Baker JE and Cremo CR (2011) Biochemistry of smooth muscle myosin light chain kinase. *Arch Biochem Biophys* **510**, 135–146.

3 Roux E, Mbikou P and Fajmut A (2012) Role of protein kinase network in excitation-contraction coupling in smooth muscle cell. In Protein Kinases (Da Silva Xavier G, ed), pp. 287–320. InTechOpen, Rijeka, Croatia.

4 Valentine KG, Ng HL, Schneeweis JK, Kranz JK, Frederick KK, Alber T and Wand AJ (2006) PDB ID: 2O5G. https://doi.org/10.2210/pdb2O5G/pdb.

5 Crouch TH and Klee CB (1980) Positive cooperative binding of calcium to bovine brain calmodulin. *Biochemistry* **19**, 3692–3698.

6 VanScyoc WS, Sorensen BR, Rusinova E, Laws WR, Alexander Ross JB and Shea MA (2002) Calcium binding to calmodulin mutants monitored by domain-specific intrinsic phenylalanine and tyrosine fluorescence. *Biophys J* **83**, 2767–2780.

7 Beccia MR, Sauge-Merle S, Lemaire D, Bremond N, Pardoux R, Blangy S, Guilbaud P and Berthomieu C (2015) Thermodynamics of calcium binding to the calmodulin N-terminal domain to evaluate site-specific affinity constants and cooperativity. *J Biol Inorg Chem* **20**, 905–919.

8 Brown SE, Martin SR and Bayley PM (1997) Kinetic control of the dissociation pathway of calmodulin-peptide complexes. *J Biol Chem* **272**, 3389–3397.

9 Fajmut A, Brumen M and Schuster S (2005a) Theoretical model of the interactions between Ca^{2+}, calmodulin and myosin light chain kinase. *FEBS Lett* **579**, 4361–4366.

10 Fajmut A, Jagodic M and Brumen N (2005b) Mathematical modeling of the myosin light chain kinase activation. *J Chem Inf Model* **45**, 1605–1609.

11 Seamon KB (1980) Calcium- and magnesium-dependent conformational states of calmodulin as determined by nuclear magnetic resonance. *Biochemistry* **19**, 207–215.

12 Ikura M, Hiraoki T, Hikichi K, Mikuni T, Yazawa M and Yagi K (1983) Nuclear magnetic resonance studies on calmodulin: calcium-induced conformational change. *Biochemistry* **22**, 2573–2579.

13 Kato S, Osa T and Ogasawara T (1984) Kinetic model for isometric contraction in smooth muscle on the basis of myosin phosphorylation hypothesis. *Biophys J* **46**, 35–44.

14 Lukas TJ (2004) A signal transduction pathway model prototype I: from agonist to cellular endpoint. *Biophys J* **87**, 1406–1416.

15 Wang I, Politi AZ, Tania N, Bai Y, Sanderson MJ and Sneyd J (2008) A mathematical model of airway and pulmonary arteriole smooth muscle. *Biophys J* **94**, 2053–2064.

16 Fajmut A and Brumen M (2008) MLC kinase/phosphatase control of Ca^{2+} signal transduction in airway smooth muscles. *Biophys J* **252**, 474–481.

17 Dabrowska R, Sherry JMF, Aromatorio DK and Hartshorne DJ (1978) Modulator protein as a component of the myosin light chain kinase from chicken gizzard. *Biochemistry* **17**, 253–258.
18 Blumenthal DK and Stull JT (1980) Activation of skeletal muscle myosin light chain kinase by calcium (2+) and calmodulin. *Biochemistry* **19**, 5608–5614.
19 Johnson JD, Snyder C, Walsh M and Flynn M (1996) Effects of myosin light chain kinase and peptides on Ca^{2+} exchange with the N- and C-terminal Ca^{2+} binding sites of calmodulin. *J Biol Chem* **271**, 761–767.
20 Wilson DP, Sutherland C and Walsh MP (2002) Activation of smooth muscle myosin light chain kinase by calmodulin. Role of LYS(30) and GLY(40). *J Biol Chem* **277**, 2186–2192.
21 Geguchadze R, Zhi G, Lau KS, Isotani E, Persechini A, Kamm KE and Stull JT (2004) Quantitative measurements of Ca^{2+}/calmodulin binding and activation of myosin light chain kinase in cells. *FEBS Lett* **557**, 121–124.
22 Gunawardena J (2012) A linear framework for time-scale separation in nonlinear biochemical systems. *PLoS One* **7**, e36321.
23 Mirzaev I and Gunawardena J (2013) Laplacian dynamics on general graphs. *Bull Math Biol* **75**, 2118–2149.
24 Gunawardena J (2014) Time-scale separation – Michaelis and Menten's old idea, still bearing fruit. *FEBS J* **281**, 473–488.
25 Dasgupta T, Croll DH, Owen JA, Vander Heiden MG, Locasale J, Alon U, Cantley LC and Gunawardena J (2014) A fundamental trade-off in covalent switching and its circumvention by enzyme bifunctionality in glucose homeostasis. *J Biol Chem* **289**, 13010–13025.
26 Ahsendorf T, Wong F, Eils R and Gunawardena J (2014) A framework for modelling gene regulation which accommodates non-equilibrium mechanisms. *BMC Biol* **12**, 102.
27 Estrada J, Wong F, DePace A and Gunawardena J (2016) Information integration and energy expenditure in gene regulation. *Cell* **166**, 234–244.
28 Tsvetkov PO, Protasevich II, Gilli R, Lafitte D, Lobachov VM, Haiech J, Briand C and Makarov AA (1999) Apocalmodulin binds to the mysoin light chain kinase calmodulin target site. *J Biol Chem* **274**, 18161–18164.
29 Romoser VA, Hinkle PM and Persechini A (1997) Detection in living cells of Ca^{2+}-dependent changes in the fluorescence emission of an indicator composed of two green fluorescent protein variants linked by a calmodulin-binding sequence. A new class of fluorescent indicators. *J Biol Chem* **272**, 13270–13274.
30 Chew T-L, Wolf WA, Gallagher PJ, Matsumura F and Chisholm RL (2002) A fluorescent resonant energy transfer-based biosensor reveals transient and regional myosin light chain kinase activation in lamella and cleavage furrows. *J Cell Biol* **156**, 543–553.
31 Isotani E, Zhi G, Lau KS, Huang J, Mizuno Y, Persechini A, Geguchadze R, Kamm KE and Stull JT (2004) Real-time evaluation of myosin light chain kinase activation in smooth muscle tissues from a transgenic calmodulin-biosensor mouse. *Proc Natl Acad Sci USA* **101**, 6279–6284.
32 Maier LS, Ziolo MT, Bossuyt J, Persechini A, Mestril R and Bers DM (2006) Dynamic changes in free Ca-calmodulin levels in adult cardiac myocytes. *J Mol Cell Cardiol* **41**, 451–458.
33 Geiser JR, van Tuinen D, Brockerhoff SE, Neff MM and Davis TN (1991) Can calmodulin function without binding calcium? *Cell* **65**, 949–959.
34 Piazza M, Taiakina V, Dieckmann T and Guillemette JG (2017) Structural consequences of calmodulin EF hand mutations. *Biochemistry* **56**, 944–956.

Supporting information

Additional supporting information may be found online in the Supporting Information section at the end of the article.
Data S1. Mathematica notebook.